Optics Letters

Orthogonal single-mode helical Bragg gratings created in fiber cladding for vector bending measurement

Baijie Xu,[1,2] Jun He,[1,2,*] Xizhen Xu,[1,2] Changrui Liao,[1,2] Xiaoyu Weng,[1] Liwei Liu,[1] Junle Qu,[1] and Yiping Wang[1,2]

[1] Key Laboratory of Optoelectronic Devices and Systems of Ministry of Education/Guangdong Province, College of Physics and Optoelectronic Engineering, Shenzhen University, Shenzhen 518060, China
[2] Shenzhen Key Laboratory of Photonic Devices and Sensing Systems for Internet of Things, Guangdong and Hong Kong Joint Research Centre for Optical Fibre Sensors, Shenzhen University, Shenzhen 518060, China
*Corresponding author: hejun07@szu.edu.cn

Received 14 November 2022; revised 7 December 2022; accepted 16 December 2022; posted 19 December 2022; published 9 January 2023

We demonstrate a novel, to the best of our knowledge, two-dimensional vector bending sensor based on orthogonal helical Bragg gratings inscribed in the cladding of a conventional single-mode fiber (SMF). The helical cladding fiber Bragg gratings (HCFBGs) are created by using a femtosecond laser direct writing technology and a quarter-pitch graded index fiber (GIF) is used in front of the HCFBGs to diverge the core mode into fiber cladding. In contrast to the multimode resonance observed in conventional cladding Bragg gratings inscribed by using a femtosecond laser point-by-point (PbP) or line-by-line (LbL) technology, the proposed HCFBGs exhibit stable narrowband single-mode Bragg resonance. An HCFBG with a low peak reflectivity of −50.77 dB and a narrow bandwidth of 0.66 nm was successfully fabricated by using a lateral offset of 45 µm between the HCFBG and the fiber core axis. Moreover, two orthogonal HCFBGs were fabricated in the SMF cladding and used for vector bending sensing. Strong orientation dependence could be seen in omnidirectional bending measurement, exhibiting a maximum bending sensitivity of up to 50.0 pm/m^{-1}, which is comparable to that in a multicore FBG. In addition, both the orientation and amplitude of bending vector could be reconstructed by using the measured Bragg wavelength shifts in two orthogonal HCFBGs. As such, the proposed HCFBGs could be used in many applications, such as structural health monitoring, robotic arms, and medical instruments.

https://doi.org/10.1364/OL.480907

Vector bending measurements are critical in many applications such as structural deformation monitoring and robotic perception [1]. Fiber Bragg gratings (FBGs) are widely developed for bending sensors due to their advantages of compact size, high sensitivity, and capability for multiplexing. In general, the core mode in an FBG is confined inside the fiber core and hence is insensitive to bending, whereas the cladding mode resonances (CMRs) are very sensitive to bending [2]. Hence, various bending sensors have been reported by using the CMRs in some specialty FBGs, such as titled FBGs, off-axis FBGs and localized FBGs [3–5]. One-dimensional (1D) bending measurements can be achieved by simply detecting the variation in the amplitude of CMRs in the FBG transmission spectra. Special mode-excitation methods, such as offset splicing, abrupt tapering, and core mismatching [6–8], are required to achieve a reflective CMR in these FBGs. However, such devices are quite complicated to assemble and typically have low mechanical strength. Moreover, two-dimensional (2D) vector bending sensing cannot be achieved using the CMRs in a single FBG. Additionally, multicore FBGs (MC-FBGs), which have narrowband reflection peaks and specially designed fiber geometry in the cross section, are invented for 2D vector bending sensing [9–13]. For example, a selectively inscribed four-core FBG was developed for 2D vector bending sensing [10]. Moreover, an array of 140 FBGs inscribed in a seven-core fiber was constructed and demonstrated for three-dimensional (3D) vector bending sensing [12]. However, fan-in/-out devices are required in these sensing systems and increase the complexity. In addition, it is challenging to efficiently inscribe high-quality FBGs on each core of the multicore fiber (MCF) [11–13]. Consequently, it is promising to develop a 2D vector bending sensor based on FBGs inscribed in a conventional single-mode fiber (SMF).

The femtosecond laser, featuring an ultra-short pulse width and an extremely high peak intensity, is a powerful tool for fabricating various FBGs in conventional SMFs [14–16]. For example, parallel-integrated FBGs (PI-FBGs) were achieved in the cross section of an SMF core and can be used for 2D bending measurements [17,18]. However, the bending sensitivity in such PI-FBGs is quite low since each FBG has a very small lateral offset (less than 2 µm) to the core axis [17]. To solve this problem, Chen *et al.* fabricated two orthogonal weak FBGs in SMF cladding with an increasing offset of 12 µm [19]. These cladding FBGs can modulate the fundamental core mode and typically have single-mode Bragg resonance in the reflection spectra. However, the lateral offset in the cladding FBGs is limited by the area of the evanescent field, and hence the bending sensitivity in such cladding FBGs will be insufficient for wavelength demodulation [20]. Instead, they used an intensity demodulation

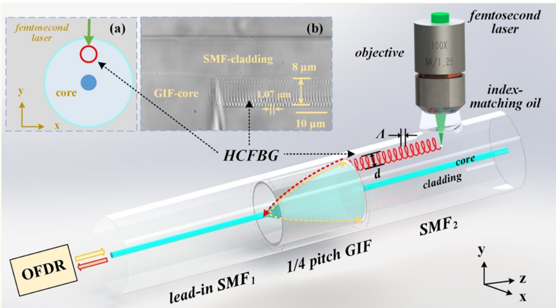

Fig. 1. Schematic of the inscription of the HCFBG in an SMF cladding by using a femtosecond laser direct-writing technology. (a) Schematic of the cross sectional view of the HCFBG; (b) side-view microscopy image of a fabricated HCFBG with a diameter of 8 μm.

scheme, which is adverse to large-scale multiplexing. Moreover, a cladding waveguide FBG (CWG) was invented to further increase the sensitivity [21,22]. The offset between the CWG and core axis was increased to 40 μm, which is comparable to that in a commercial MCF. Hence, the CWG exhibits a similar bending sensitivity (42.4 pm/m^{-1}) to an MC-FBG. Nevertheless, an extra femtosecond laser directly inscribed single-mode waveguide was required to couple the light from the fiber core to CWG and the fabricated CWG was susceptible to external refractive index perturbations [23].

In this Letter, we propose and demonstrate a novel 2D vector bending sensor in a conventional SMF by directly inscribing a pair of orthogonal helical Bragg gratings in the cladding via a femtosecond laser. In our previous work [24], we have shown that such a helical structure in a multimode coreless fiber can operate both as a single-mode waveguide and also as a periodic Bragg grating. Hence, the proposed helical cladding fiber Bragg grating (HCFBG) can also generate narrowband single-mode Bragg resonance. In addition, a quarter-pitch graded index fiber (GIF) was added in front of the HCFBG to diverge the core mode into the cladding [25]. Hence, the offset between the HCFBG and fiber core axis was increased to 45 μm, leading to a high bending sensitivity up to 50.0 pm/m^{-1}, which is comparable to that in a multicore FBG. Furthermore, 2D vector bending measurements were also achieved by using the measured Bragg wavelength shifts in two orthogonal HCFBGs.

Figure 1 shows the setup for fabricating the HCFBGs by using a femtosecond laser direct writing technology. The setup employed a frequency-doubled regenerative amplified Yb:KGW [KGd(WO_3)] femtosecond laser (Pharos, Light-conversion) with a wavelength of 514 nm, a pulse width of 290 fs, and a repetition rate of 200 kHz. A Leica oil-immersion objective (100×, N.A. = 1.32) was used as the focusing element. Moreover, reflective index oil (n = 1.4587) was applied to mitigate the aberration induced by the fiber cylindrical geometry. The optical fiber was fixed by a pair of fiber holders mounted on a 3D air-bearing translation stage (assembled by Aerotech ABL15010, ANT130LZS, and ANT130V-5). In addition, a commercial optical frequency domain reflectometer (OFDR; LUNA, OBR4600) was used for interrogating the fabricated HCFBG sample, which typically has extremely low peak reflection of approximately −50 dB [15].

The process for inscribing an HCFBG is also shown in Fig. 1. At first, a quarter-pitch GIF (YOFC, GI 100/125) with a length of 400 μm was spliced with two SMFs (i.e., SMF_1 and SMF_2) to form an SMF-GIF-SMF structure. The quarter-pitch GIF functions as an in-fiber collimator to expand the beam incident into the HCFBG. Then, the fiber sample was mounted on the translation stage and the fiber axis was adjusted parallel to the z axis. Then, the shutter was opened, and the femtosecond laser beam was focused into the cladding of SMF_2. During this process, the sample was translated in a helical trajectory via synchronous movements along the x, y, and z axes. Hence, a helical Bragg grating was successfully fabricated in the SMF_2 cladding. As shown in Fig. 1(a), the cross section of the helical structure is annular, which serves as a depressed cladding. Moreover, as shown in Fig. 1(b), the HCFBG exhibits a diameter of $d = 8$ μm and a helical pitch of $\Lambda = 1.07$ μm, and can yield Bragg resonance in the telecommunication C-band. The working principle of the proposed HCFBG is also illustrated in Fig. 1. A partial incident core mode is coupled to the downstream SMF cladding and excites cladding modes through the GIF. Then, the unique helical structure serves as a depressed cladding waveguide and can reflect a single-mode Bragg resonance back into the GIF, and finally to the upstream SMF.

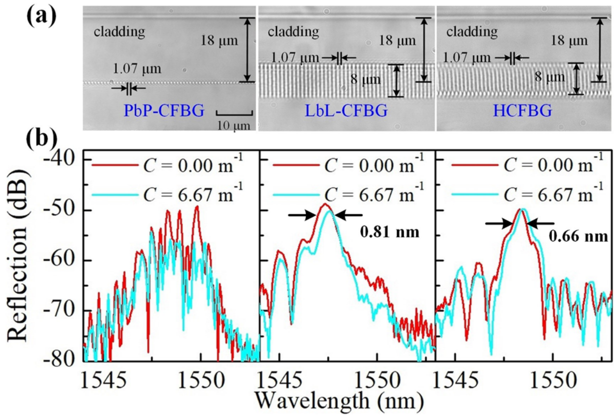

Fig. 2. (a) Microscopy images and (b) reflection spectra of a PbP-FBG, a LbL-FBG, and an HCFBG fabricated in the SMF cladding by femtosecond laser direct-writing technology with the same grating pitch of 1.07 μm, the same grating length of ∼2 mm, and the same offset of ∼45 μm.

At first, three different types of FBGs, i.e., point-by-point FBG (PbP-FBG), line-by-line FBG (LbL-FBG), and HCFBG, were inscribed in the cladding of the SMF by using a femtosecond laser direct-writing technology. As shown in Figs. 2(a1)–2(a3), the three FBGs have the same grating pitch of 1.07 μm, the same grating length of ∼2 mm, and the same offset of ∼45 μm between the grating axis and fiber core axis. The LbL-FBG has a track length of ∼8 μm, approaching to the diameter of the HCFBG. In the case of the PbP-FBG, as shown in Fig. 2(b1), multiple peaks (corresponding to Bragg resonances of high-order modes) and a large bandwidth are observed in the reflection spectrum. Moreover, in the case of the LbL-FBG, as shown in Fig. 2(b2), a reduced bandwidth of 0.81 nm is obtained since the higher-order modes are partially suppressed. However, in the case where the PbP-FBG and LbL-FBG samples are bent with a curvature of 6.67 m^{-1}, as shown in Figs. 2(b1) and 2(b2), the bandwidth is slightly reduced, and the peak reflectivity decreases obviously. This mainly results from the increasing loss of high-order modes when FBGs fabricated in the SMF cladding are bent. However,

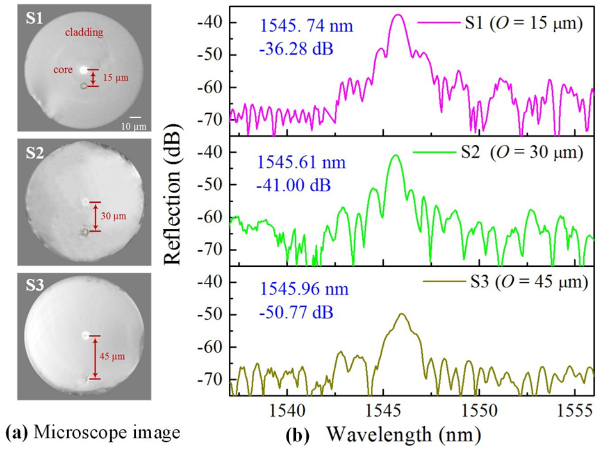

Fig. 3. (a) Cross sectional microscopy images and (b) reflection spectra of three fabricated HCFBGs S1–S3 with increasing offset of 15, 30, and 45 μm, respectively.

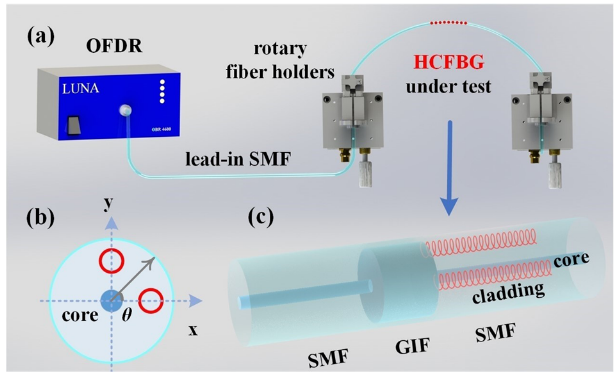

Fig. 4. (a) Experimental setup for 2D vector bending measurement by using the HCFBG; (b) schematic of cross sectional view and (c) 3D schematic of the orthogonal HCFBGs.

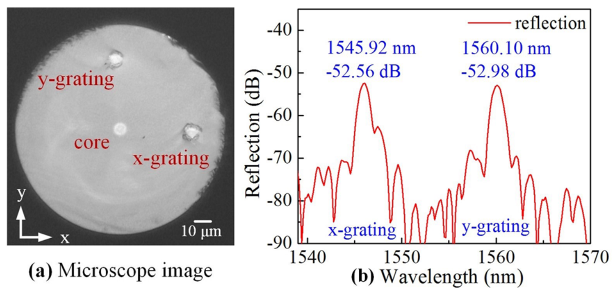

Fig. 5. (a) Cross sectional microscopy image and (b) reflection spectra of the two fabricated orthogonal HCFBGs.

in the case of the HCFBG, as shown in Fig. 2(b3), a high-quality reflection spectrum is obtained, showing pure single-mode Bragg resonance with a narrow bandwidth of 0.66 nm. Moreover, the reflection spectrum of the HCFBG shows a "red" shift after bending, whereas the peak intensity and the bandwidth hardly change. This may result from the single-mode waveguide created in the HCFBG, indicating the fabricated HCFBG will be very suitable for highly stable bending measurements.

Subsequently, three different HCFBG samples, i.e., S1, S2, and S3, were inscribed in the SMF cladding with increasing offset between the HCFBG and fiber core axis of 15, 30, and 45 μm by using the same pulse energy of 10 nJ. Note that the HCFBGs have the same length of 2 mm, the same helical diameter of 8 μm, and the same helical pitch of 1.07 μm. As shown in Fig. 3(a), three ring-shape patterns with different offset are created in the cross section of HCFBGs. As shown in Fig. 3(b), the fabricated HCFBGs S1–S3 have a similar Bragg wavelength of 1545.74, 1545.61, and 1545.96 nm, respectively, but the peak reflectivity decreases as the offset increases from S1 to S3. In the case where the offset increases to 45 μm, the reflection can still be detected, and the grating exhibits a low peak reflectivity of −50.77 dB. Note that the offset is similar to the spacing between the outer core and central core in the SCF.

Furthermore, we studied the 2D vector bending response of the HCFBG by using the experimental setup shown in Fig. 4(a). A commercial OFDR was used to simultaneously interrogate the wavelengths of all HCFBGs fabricated in the SMF. Note that no fan-in/-out devices were required to demodulate the HCFBGs. The HCFBG sample was fixed in place by a pair of rotary fiber holders and mounted on a bending calibration plate, which was engraved with a set of arc grooves with preset curvatures ranging from 6.67 to 20 m^{-1}. The bending direction was preset by synchronously rotating two fiber holders, avoiding the fiber torsion during bending measurement. In specific, the bending orientation angle θ was defined as the included angle between the bending plane and x axis, as shown in Figs. 4(b) and 4(c). When $\theta = 0°$ or 360°, the SMF was bent along the x axis, and the x-grating was located on the inner side of the bent SMF. When $\theta = 180°$, the SMF was again bent along the x axis, but the x-grating was located on the outer side of the bent SMF. The initial angle alignment of the sample can be carried out by rotating the fiber holders according to the microscopy images captured by a CCD camera in real-time. Moreover, the wavelength shifts were recorded for each HCFBG at varying bending orientations.

It should be noted a single HCFBG can achieve only 1D vector bending and cannot be used for 2D vector bending measurements. Two orthogonal FBGs are required to realize 2D vector sensing by detecting bending components along two directions. Consequently, as shown in Figs. 4(b) and 4(c), we inscribed two orthogonal HCFBGs in the SMF cladding by femtosecond laser direct-writing technology to obtain the horizontal (x) and vertical (y) bending components. The first HCFBG, i.e., x-grating, was fabricated in the SMF cladding by using a helical pitch of 1.07 μm and the same fabrication parameters as the sample in Fig. 3 (i.e., a pulse energy of 10 nJ and a grating length of 2 mm). The SMF was then azimuthally rotated by 90°, and another HCFBG, i.e., y-grating, was sequentially inscribed in the SMF cladding with a different helical pitch of 1.078 μm. Both x- and y-gratings were set to 45 μm away from the fiber core axis. As shown in Fig. 5(a), two orthogonal ring-shaped inscription patterns could be seen clearly in the cross section of the fabricated HCFBGs. As shown in Fig. 5(b), two HCFBGs had a distinct peak wavelength of 1545.92 and 1560.10 nm, and a similar peak reflectivity of −52.56 and −52.98 dB, respectively.

We tested the bending sensitivities of the fabricated HCFBGs in different bending directions and curvature. The wavelength shifts of x- and y-gratings were recorded at various orientation angles θ from 0° to 360° in a step of 15° and the test was repeated under different bending curvature from 6.67 to 20.0 m^{-1}. As shown in Fig. 6(a), in the case where the HCFBG locates at the outer side of the bent fiber, it will be stretched and exhibits a "red" shift. In contrast, in the case where the

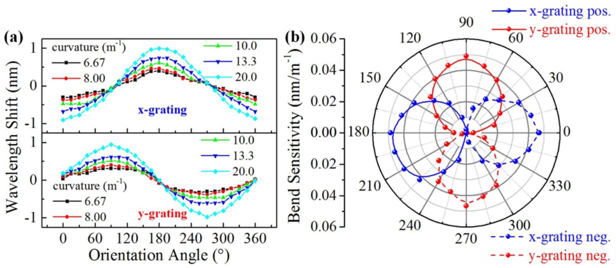

Fig. 6. (a) Measured Bragg wavelength shift of both orthogonal HCFBGs as functions of bending orientation angle θ under different curvatures; (b) bending sensitivities of the orthogonal HCFBGs plotted for various bending directions in polar coordinates.

HCFBG locates at the inner side of the bent fiber, it will be compressed and exhibits a "blue" shift. Note that all wavelength shifts for a given curvature exhibit good agreements with sinusoidal curves and the responses of wavelength shift to curvature are different in various directions. Linear fits were applied to all Bragg wavelength shifts of both x- and y-gratings at various orientation angles θ from 0° to 360°. Hence, the bending sensitivities of x- and y-gratings were obtained and drawn in polar coordinates. As shown in Fig. 6(b), two perfect "8"-shaped patterns corresponding to x- and y-gratings are observed, and each "8"-shaped pattern includes two maxima and two minima. The highest sensitivities are achieved when the fiber is bent along the axis connecting the HCFBG and the fiber core, whereas the lowest sensitivities occur when the fiber is bent in the orthogonal direction. The maximum sensitivities of the HCFBGs in the x- and y- direction were 50.0 and 49.5 pm/m^{-1} at an orientation angle θ of 180° and 90°, respectively. The sensitivity of each HCFBG fluctuates slightly due to the errors in the rotation angles during the bending measurement. Therefore, 2D vector bending sensing, including orientation and amplitude, could be achieved by using the measured wavelength shifts of two HCFBGs and orthogonal position relationship between them.

In summary, we have demonstrated a novel 2D vector bending sensor based on two orthogonal HCFBGs inscribed in the cladding of the SMF. An HCFBG was fabricated to generate a single-mode Bragg resonance. A quarter-pitch GIF was added in front of the HCFBGs to diverge the core mode into the fiber cladding and hence could increase the offset between HCFBGs and the fiber core axis. As a result, the offset was increased to 45 µm, leading to a maximum bending sensitivity of HCFBGs of up to 50 pm/m^{-1}. Furthermore, a pair of orthogonal HCFBGs were successfully fabricated in the SMF cladding by using the same fabrication parameters and were then used for 2D bending measurement. As such, the proposed HCFBGs will be very useful in many applications, such as structural health monitoring, robotic arms, and medical instruments.

Funding. National Natural Science Foundation of China (62222510, U1913212, 62005170); Guangdong Science and Technology Department (2019TQ05X113, 2022B1515120050); Science and Technology Innovation Commission of Shenzhen (JCYJ20210324120403009, RCYX20200714114538160).

Disclosures. The authors declare no conflicts of interest.

Data availability. Data underlying the results presented in this paper arenot publicly available at this time but may be obtained from the authors upon reasonable request.

REFERENCES

1. H. Wang, R. Zhang, W. Chen, X. Liang, and R. Pfeifer, IEEE/ASME Trans. Mechatron. **21**, 2977 (2016).
2. L. Y. Shao, L. Xiong, C. Chen, A. Laronche, and J. Albert, J. Lightwave Technol. **28**, 2681 (2010).
3. L. Xie, B. Luo, M. Zhao, O. Deng, E. Liu, P. Liu, Y. Wang, and L. Zhang, Opt. Lett. **45**, 125 (2020).
4. D. Feng, X. Qiao, and J. Albert, Opt. Lett. **41**, 1201 (2016).
5. J. He, R. Chen, X. Xu, J. He, B. Xu, S. Liu, C. Liao, D. Liu, Y. Gong, and Y. Wang, J. Lightwave Technol. **40**, 5722 (2022).
6. Q. Rong, X. Qiao, H. Yang, K. S. Lim, and H. Ahmad, IEEE Photonics Technol. Lett. **27**, 1108 (2015).
7. W. Cui, J. Si, T. Chen, and X. Hou, Opt. Express **23**, 11031 (2015).
8. T. Guo, A. Ivanov, C. Chen, and J. Albert, Opt. Lett. **33**, 1004 (2008).
9. G. M. Flockhart, W. N. MacPherson, J. S. Barton, J. D. Jones, L. Zhang, and I. Bennion, Opt. Lett. **28**, 387 (2003).
10. W. Bao, N. Sahoo, Z. Sun, C. Wang, S. Liu, Y. Wang, and L. Zhang, Opt. Express **28**, 26461 (2020).
11. M. Hou, K. Yang, J. He, X. Xu, S. I. Ju, K. Guo, and Y. Wang, Opt. Express **26**, 23770 (2018).
12. X. Xiao, B. Xu, X. Xu, B. Du, Z. Chen, C. Fu, C. Liao, J. He, and Y. Wang, Opt. Lett. **47**, 758 (2022).
13. C. Liu, Y. Jiang, J. Li, B. Du, X. Liao, J. Wang, and D. Yang, Opt. Lett. **47**, 4000 (2022).
14. J. He, B. Xu, X. Xu, C. Liao, and Y. Wang, Photonic Sens. **11**, 203 (2021).
15. B. Xu, J. He, B. Du, X. Xiao, X. Xu, C. Fu, J. He, C. Liao, and Y. Wang, Opt. Express **29**, 32615 (2021).
16. F. Chen, X. Li, R. I. Wang, and X. Qiao, Opt. Lett. **47**, 786 (2022).
17. Y. Wang, Z. Li, S. Liu, C. Fu, Z. Li, Z. Zhang, Y. Wang, J. He, Z. Bai, and C. Liao, J. Lightwave Technol. **37**, 2185 (2019).
18. K. Guo, J. He, H. Li, B. Xu, S. Lu, S. Liu, X. Xu, G. Xu, and Y. Wang, J. Lightwave Technol. **40**, 2166 (2022).
19. F. Chen, X. Li, R. Wang, and X. Qiao, Opt. Lett. **46**, 2992 (2021).
20. F. Chen, X. Li, R. Wang, and X. Qiao, J. Lightwave Technol. **39**, 1 (2021).
21. C. Waltermann, A. Doering, M. Kohring, M. Angelmahr, and W. Schade, Opt. Lett. **40**, 3109 (2015).
22. K. K. Lee, A. Mariampillai, M. Haque, B. A. Standish, V. X. Yang, and P. R. Herman, Opt. Express **21**, 24076 (2013).
23. C. Lin, C. Liao, J. Wang, J. He, Y. Wang, Z. Li, T. Yang, F. Zhu, K. Yang, Z. Zhang, and Y. Wang, Opt. Lett. **42**, 1684 (2017).
24. J. He, J. He, X. Xu, B. Du, B. Xu, C. Liao, Z. Bai, and Y. Wang, Photonics Res. **9**, 2052 (2021).
25. X. Xu, J. He, M. Hou, S. Liu, Z. Bai, Y. Wang, C. Liao, Z. Ouyang, and Y. Wang, J. Lightwave Technol. **36**, 2827 (2018).